Journal of
Ceramic Science
and Technology

J. Ceram. Sci. Technol., **09** [1] 7-18 (2018)
DOI: 10.4416/JCST2017-00049
available online at: http://www.ceramic-science.com

Effects of Stabilizer Content and Sintering Conditions on Y-TZP Ceramics made from Stabilizer-Coated Nanopowders

F. Kern*, H. Strumberger, R. Gadow

University of Stuttgart, Institute for Manufacturing Technologies of Ceramic Components and Composites, Allmandring 7B, D-70569 Stuttgart, Germany

received July 3, 2017; accepted September 12, 2017

Abstract

Yttria-stabilized zirconia Y-TZP according to the state of the art has become a commodity applied in mechanical engineering and biomedicine. Besides the high strength typical for Y-TZP, the improved damage tolerance and fatigue strength are beneficial for components exposed to cyclic stress. In this study, Y-TZP materials were produced by means of hot pressing of nanoscale powders coated with yttria via a wet chemical route. Stabilizer contents were varied from 2.6 – 3 mol% Y_2O_3; sintering was carried out between 1250 °C and 1450 °C and 50 MPa axial pressure for 1 h. Samples were characterized in respect of their microstructure, phase composition and mechanical properties. Hardness and strength rise with stabilizer content and sintering temperature while fracture resistance showed a more complex dependence on composition and heat treatment parameters. Toughness in general declines from a comparable maximum level of 10 – 11 MPa√m at 1300 °C with rising sintering temperature, the decline is more pronounced for samples with high stabilizer content.

Keywords: Zirconia, phase composition, microstructure, mechanical properties

I. Introduction

The excellent mechanical properties of zirconia-based structural ceramics are based on transformation toughening [1,2]. Transformation toughening occurs when metastable tetragonal zirconia incurs a stress-induced martensitic transformation to stable monoclinic phase. This happens e.g. at the tip of a crack under stress. The phase transformation takes place at the speed of sound in the material and is associated with a volume expansion ε_T of 5 % and shear. A proceeding crack is thus put under compressive stress from both sides, the transformation toughening effect depends on the amount of zirconia transformed, the depth of the transformation zone, and a coefficient X describing transformation efficiency, which can vary from 0.22 for purely dilatation to 0.48 for dilatation and shear [2]. In Y-TZP, owing to the small grain size of the material and crystallographic boundary conditions impeding the growth of monoclinic domains from one grain into another, the toughening effect reaches its saturation limit after a short crack length so that these materials typically have an extremely steep R-curve [3,4]. The typical stabilizer contents in Y-TZP range from 2.5 – 3.5 mol% yttria [2]. At sintering temperatures typically ranging from 1300 – 1550 °C these compositions are thus located in the t+c field, which marks a miscibility gap [5]. For thermodynamic reasons, these compositions should segregate into a stabilizer-rich cubic fraction with a composition at the t+c/c phase boundary (6 – 7 mol% yttria) and a stabilizer-poor tetragonal fraction having yttria contents in the range between 2.4 and 2.6 mol% [5]. Addition of aliovalent Y^{3+} ions implies formation of oxygen vacancies to retain charge neutrality and brings zirconia into a sevenfold coordination in the tetragonal polymorph [6]. The state-of-the-art technology to produce Y-TZP powders is coprecipitation of zirconia and yttria precursors leading to perfect distribution of stabilizer on atomic level as it was an accepted dogma that only powders of perfect homogeneity can lead to good mechanical properties and ageing resistance [7]. As the typical 3 mol% yttria-stabilized zirconia is initially entirely tetragonal but supersaturated with yttria, there is a trend for yttria to be accumulated at the grain boundary (solute drag) [8]. The phase separation requires high temperatures and dwell owing to the fact that phase separation and formation of cubic is an "uphill diffusion" process against the concentration gradient [9]. The solute drag effect is, however, also the reason why Y-TZP shows only limited grain growth during sintering [8]. Upon cooling from sintering temperature and passing the eutectoid line at ~ 1100 °C, the tetragonal (+cubic) material should decompose to monoclinic and cubic [5]. This thermodynamic stable composition is, however, avoided with sufficiently high cooling rates so that the tetragonal phase is retained metastable at room temperature and is available for the transformation toughening effect. Besides the stress-induced transformation, a spontaneous transformation may occur with the incorporation of polar molecules (typically hydroxyl species) into the oxygen vacancies, this effect called low-temperature degrada-

* Corresponding author: frank.kern@ifkb.uni-stuttgart.de

tion (LTD) and occurs when Y-TZP comes into contact with water and destabilizes the tetragonal phase [10]. LTD is not the subject of this paper. Typical state-of-the-art 3Y-TZP materials can reach a bending strength beyond 1000 MPa and fracture resistance values between 4.5 and 6 MPa√m [11,12]. Taking into account the low resistance to subcritical crack growth of 2.8 MPa√m under atmospheric conditions, the fatigue strength is only about half the bending strength, which may become critical in dental applications as mastication forces may reach 600 MPa [13,14]. In order to improve the fracture resistance of coprecipitated Y-TZP, two strategies have been proposed, lowering the stabilizer content to increase the metastability of the tetragonal phase and increasing the sintering temperature to obtain larger grain sizes and promote phase separation, both issues, however, make the materials more vulnerable to spontaneous failure and limit maximum strength [11,15]. Recently, Danilenko reported on improved fracture resistance in 3Y-TZP that was coprecipitated together with a small amount of alumina and reaches higher fracture resistance at relatively low transformability. The effect is most likely caused by residual stress effects of intragranular alumina [16]. Y-TZP materials made by means of wet-chemical coating of unstabilized zirconia powders with stabilizer or intensive co-milling of zirconia with stabilizer have been studied by several authors. The technology dates back to the time when no coprecipitated powders were available [17], materials with attractive properties were first reported by Lawson, Singh and Burger using powder from the British company Tioxide which was manufactured from plasma-atomized zirconia intensively co-milled with yttria [18,19]. Yuan introduced a viable coating process starting from yttrium nitrate [20]. Ohnishi reported on materials made by intensive co-milling of zirconia and stabilizer [21]. Recently this technology was also applied to process ultrafine powders and to introduce other rare earth oxides or combinations of different stabilizers [22,23,24]. With the use of coated powders, much higher fracture resistance values can be obtained in Y-TZP than with the use of coprecipitated starting materials. There is, however, an inversion of grain size-toughness correlations at high sintering temperatures, this effect was first reported by Singh [19]. The reasons for the outstanding toughness of these materials was controversially discussed in the past. While one group argued for a broadening of the grain size distribution, the other group was in favor of a stabilizer gradient model [25,19]. Both effects were found in 2.5Y-TZP depending on sintering temperature by the authors [26]. Still it seems that in case of TZPs with ultrafine microstructure experimental evidence is in favor of the gradient model. It is assumed that initially all stabilizer is located outside the monoclinic grains and diffuses into the grains in the course of the sintering process. Thereby the cores of the grains are initially unstabilized and become successively enriched in yttria with proceeding time and increasing temperature. As the t+c field is a miscibility gap, the bulk of the grains cannot take up more than the thermodynamic equilibrium, the grain boundary may accommodate more stabilizer [9]. Hence contrary to the situation in the coprecipitated powder in which the grains are initially supersaturated, the phase separation can take place without uphill diffusion. Thus it seems that at moderate sintering temperatures, where high toughness is observed, the grain boundaries are supersaturated while the bulk is understabilized. The onset of transformation starts, however, at the grain boundaries so that starting transformation requires high stress (i.e. the strength of the materials is higher than can be expected from classical strength toughness correlations), once the transformed region extends to the core, the high transformability of the understabilized zirconia provides high toughness. In this study, an experimental plan covering the typical range of stabilizer concentration (2.6 – 3 mol% Y_2O_3) and sintering temperatures (1250 °C – 1450 °C) was developed to deliver further evidence for this interpretation.

II. Experimental

Material synthesis started from agglomerated granules of 0.4 μm diameter of a nanoscale unstabilized zirconia powder with a specific surface area of S_{BET} = 15 m²/g. A stabilizer coating process was carried out according to a procedure described by Yuan and previously modified by the authors [20,27]. The zirconia was dispersed in 1500 ml 2-propanol in a 2000-ml polyethylene bottle. Yttrium oxide (99.9 % purity) was dissolved in boiling 5N nitric acid. The cooled nitrate solution was then added to the zirconia dispersion. Four batches of 500 g (zirconia + yttria) containing 3 mol%, 2.85 mol%, 2.7 mol% and 2.6 mol% were prepared (denoted as 2.6Y, 2.7Y, etc.). After gentle milling overnight in the PE bottle with Y-TZP balls of 2 mm diameter, the milling media were separated and the resulting dispersion was dried overnight in air at 90 °C. The resulting material was then heat-treated in air at 350 °C for 3 h to decompose the nitrate. The lump of pre-calcined powder was ground with mortar and pestle and passed through a 200-μm screen before final calcination at 600 °C for 3 h in air. 0.5 vol% submicron size alumina (d_{50} = 300 nm) was added to the powders. The blend was then attrition-milled in 2-propanol for 2 h at 400 rpm with Y-TZP balls to break down the agglomerates. After being dried in air at 1350 °C and another screening operation using a 100-μm mesh, the powder was ready for further processing. The samples were consolidated by means of hot pressing in a graphite die for 1 h at 50 MPa axial pressure (FCT Anlagenbau, Germany). Two disks with a diameter of 45 mm and a thickness of 2.3 mm were sintered from all four stabilizer contents at 1250 – 1400 °C in 50 K increments. This results in 20 different types of materials. After heating to 1150 °C at 30 K/min and 3 kN pre-load, the load was increased to 32 kN (~ 20 MPa) within a 10-min dwell, then heating to final sintering temperature was continued at 50 K/min while the pressure was increased to 50 MPa. After 1-h dwell at final temperature and pressure, the heater was switched off, the furnace chamber was filled with argon and the samples were cooled down to ambient temperature in the press.

The resulting disks were machined on both sides by means of lapping and polishing to a mirror-like finish with 15-μm, 6-μm, and 1-μm diamond suspension (Struers Rotopol, Denmark). Density was determined with the buoyancy method; Young's modulus E, shear modulus G and Poisson's ratio ν were measured with the reso-

nance frequency method (EMCE, Belgium) on two entire disks each. The disks were then cut into bars measuring 4 mm in width, which were subsequently lapped on the sides to remove cutting grooves. The edges were carefully beveled using a 40-µm diamond disk. 14 test bars were obtained for each composition. Hardness HV10 was measured (Bareiss, Germany, 5 – 10 indents each). Bending strength was measured in a 4pt setup with 20-mm outer and 1-mm inner span and a crosshead speed of 0.5 mm/min (Zwick, Germany, 10 samples). Fracture resistance was measured in the same setup (4 samples) using the indentation strength in bending test (ISB). Bending bars were notched with HV10 indents in the middle of the tensile side with cracks parallel and perpendicular to the sides and residual strength was measured immediately after that at a crosshead speed of 2.5 mm/min. The fracture resistance was calculated according to Chantikul [28]. In addition to that, stable indentation crack growth in bending (SIGB) experiments were carried out at 5 mm/min following a procedure described by Dransmann [29]. The bending bars were first indented with four HV10 indents aligned lengthwise at a distance of 2 mm in the middle of the tensile side. The samples were then left to rest for two weeks to develop a stable initial crack length. Then the samples were loaded with increasing loads until fracture and crack length was measured after each loading step using the microscope of the hardness tester. Based on previous experience with the method, measuring parameters for SIGB were chosen individually for all samples [24, 27]. Starting from a value 30 % of the ISB residual strength, the load increase per step was set at 10 % of ISB strength for each individual sample. As the indenter exerts a certain stress intensity, the negative value of this stress intensity – $K_{app,0}$ is stored in the sample when the indenter is lifted. In the bending test, the crack starts to grow once the applied stress intensity K_{app} equals or surmounts this value. The measured crack length is then plotted against the applied stress intensity. In a characteristic SIGB plot $\Psi \cdot \sigma \cdot \sqrt{c}$ (Ψ = 1.27 geometry factor; σ = applied bending stress; c = crack length from indent center to crack tip) is plotted vs. $P \cdot c^{-1.5}$ (P = 98.1 N indent load). The plot has two sections: if $K_{app} < K_{app,0}$ then $P \cdot c^{-1.5}$ increases at identical $\Psi \cdot \sigma \cdot \sqrt{c}$. After it starts to grow, the curve kinks and a linear segment follows with a slope χ which denotes the residual stress coefficient. The extrapolation of this linear part leads to the ordinate intercept K_{IC}, a fracture toughness value at infinite crack length. The resistance to subcritical crack growth = threshold toughness K_{I0} is the difference between K_{IC} and $K_{app,0}$ [29]. Lube and Fett have, however, shown that the extrapolation may lead to overestimated toughness values [30]. Further comments on toughness measurements will follow in the results and discussion sections. The phase composition of the samples was measured with XRD (Bruker D8, Germany, Bragg-Brentano-setup, CuKα). According to the calibration curve by Toraya, intensities of the three characteristic reflections $(-111)_m$, $(111)_m$ and $(101)_t$ in the 2theta range between 27 – 33°C were measured and evaluated [31]. First polished disks were measured to determine the monoclinic content $V_{m,pol}$ in the bulk material, then monoclinic contents in fracture faces $V_{m,FF}$ of ISB samples were measured to determine the transformed fraction V_f ("transformability") during fracture. Based on these data, transformation zone depths h were calculated according to Kosmac and transformation toughness increments $\Delta K_{IC}{}^T = X \cdot 1/(1-\nu) \cdot E \cdot \varepsilon_T \cdot V_f \cdot \sqrt{h}$ were calculated according to McMeeking and Evans using a typical value of X = 0.27 for Y-TZP (predominantly dilatoric) and ε_T = 0.05 (volume change during t-m transformation) [32, 33]. Fracture faces and polished, thermally etched (1200 °C, 5 min in hydrogen) samples were studied with SEM (Zeiss Gemini, in lens technology, secondary electrons 3kV, PtPd coated samples) to analyse microstructure and measure grain sizes with the linear intercept method (measured average values multiplied by 1.54 to compensate off-center intersections). In addition to that, the fracture faces of ISB samples were studied by means of microscopy (Leica, Germany), uplift around indents caused by deformation and transformation was documented with microscopy using differential interference contrast (DIC) and measured by means of white light interferometry (Bruker, Germany).

Calculation of errors and standard deviations: Depicted errors correspond to standard deviations of measurements for HV10 (5 – 10 indents), σ_{4pt} (10 samples), K_{ISB} (4 – 6 samples), uplift by white light interferometry (5 indents) and average grain size (4 lines across a SEM image of 20000x magnification). Errors of monoclinic contents correspond to standard errors for integration of the three characteristic reflections and their propagation (largest error in determination of $V_{m,pol}$). The errors in determination of density are weighing errors, which were minimized by testing two entire disks of 20 g at an accuracy of 0.001 g, water temperature was measured at 0.1 °C. SIGB-based fracture resistance values (errors not displayed in the graphs for sake of clarity) were tested on 2 bars each (i.e. 8 indents, 6 survivors in the final loading step). Determination of $K_{app,0}$ was carried out graphically, accuracy is ± 0.2 MPa$\sqrt{m}$, which adds to the standard deviations of K_{ISB} for determination of K_{I0}. Calculated values of h and $K_{IC}{}^T$ (standard deviations not displayed in the graphs) include many measured variables and their error propagation with the largest errors coming from the XRD data, here the total error exceeds 25 %.

III. Results

(1) Mechanical properties

Density and elastic modulus values vary around the typical value of ϱ = 6.05 – 6.1 g/cm³ and E = 205 – 210 GPa [11, 12]. Typically between 1250 – 1300 °C, density rises by only 0.02 g/cm ~ 0.3 %, thus all materials can be considered fully dense. Elastic modulus shows a slight initial increase in the order of the standard deviation of ± 3 – 4 GPa. Poisson's ratio fluctuates slightly around literature values of 0.31 ± 0.01 [12]. Fig. 1 shows the Vickers hardness HV10 of the materials depending on stabilizer content and sintering temperature. Hardness rises almost linearly between sintering temperatures of 1250 – 1400 °C; then the trend levels out. Higher stabilizer contents favor higher hardness values. The bending strength of the

materials is shown in Fig. 2. Bending strength and hardness show almost identical trends. Starting from values of 750 – 800 MPa at the lowest sintering temperature, the strength rises continuously, the increase in strength is more pronounced in materials containing high stabilizer amounts (1250 MPa at 1450 °C for 3Y, 950 – 1000 MPa for 2.6Y and 2.7Y at the same temperature). The fracture resistance determined based on indentation strength in bending ISB is shown in Fig. 3. Toughness shows an inverse trend to strength and hardness. The highest toughness values of 10 – 12 MPa√m are generally obtained at low sintering temperatures < 1350 °C. 2.85Y and 3Y show their toughness maximum at 1350 °C and 1300 °C respectively. For these compositions containing high amounts of stabilizer, a drastic decline in toughness to a level of K_{ISB} = 6 – 7 MPa√m is observed at sintering temperatures ≥ 1400 °C. It seems that 2.6Y and 2.7Y are less vulnerable in respect of high sintering temperatures. Fracture resistance of 2.7 shows a flat profile while 2.6Y shows a decline in toughness only at the highest sintering temperature.

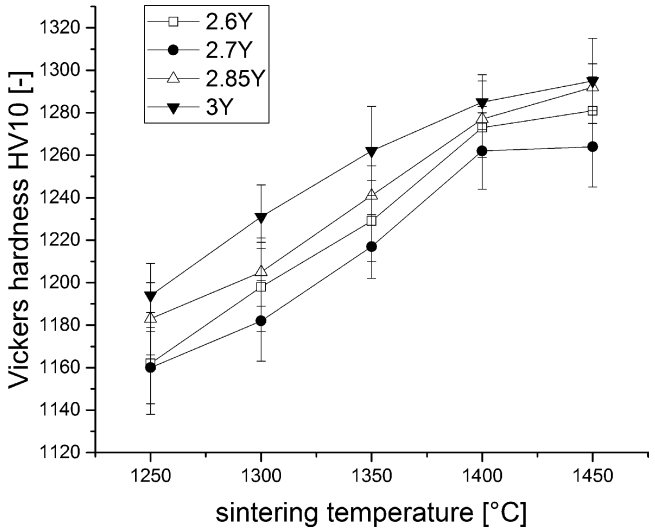

Fig. 1: Vickers hardness HV10 of the Y-TZPs depending on stabilizer content and sintering temperature.

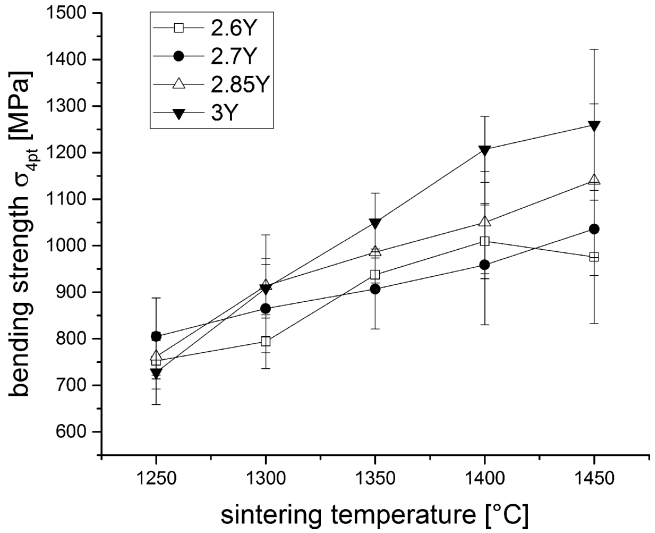

Fig. 2: Bending strength σ_{4pt} of the Y-TZPs depending on stabilizer content and sintering temperature.

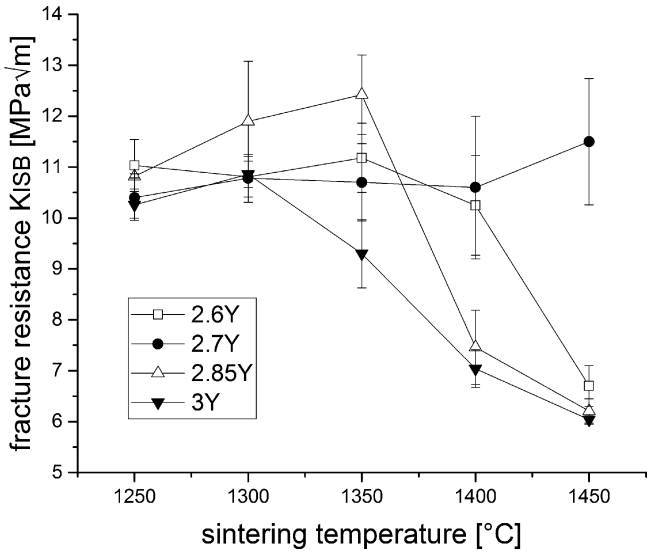

Fig. 3: Fracture resistance K_{ISB} determined by indentation strength in bending method of the Y-TZPs depending on stabilizer content and sintering temperature.

The choice of measurement protocol for fracture resistance determination in transformation-toughened materials is the subject of controversial discussion. In order to demonstrate the limits of different methods, some examples for surface and subsurface structure of indents and indentation-based cracks and surface uplift are given in Figs. 4 – 6. In Fig. 4, three characteristic examples for HV10 indents in different materials are given. At low stabilizer content and sintering temperature (2.6Y-1250 °C) a strong and quite irregular transformation zone around the indent is formed. Finger-like transformation zones extending relatively far into the surrounding area can be seen, indentation-based cracks are non-uniformly shaped and predominantly trapped within the transformation zones. At intermediate sintering temperatures and increased stabilizer content (3Y-1350 °C) the transformation and uplift are still significant but become uniform. Indentation cracks extend almost to the verge of the transformation zone but are still embraced by transformation bands. Only at the highest sintering temperatures do the crack patterns become entirely regular. Uplift zones are visible but not very pronounced and cracks extend far beyond the sphere of influence of the transformed region. In Fig. 5 the quantitative information on uplift around the HV10 indentations is given, the height of the uplifted zone was measured by means of white light interferometry. Generally, the uplift declines linearly with increasing sintering temperature from 1.45 – 1.7 µm at 1250 °C to 0.9 – 1.1 µm at 1450 °C. As the hardness of all the materials is not too different and the displaced volume should thus be similar, the largest part of uplift must be caused by the volume expansion associated with phase transformation. Fig. 6 shows that even at the highest sintering temperature and stabilizer contents (3Y-1450 °C) the cracks are Palmqvist type. Owing to the existence of a plastified zone below the indent, the cracks grow preferentially in lateral direction, forming an inclined B-shaped pattern. For the samples sintered at lower temperature (3Y-1300 °C), the two lobes

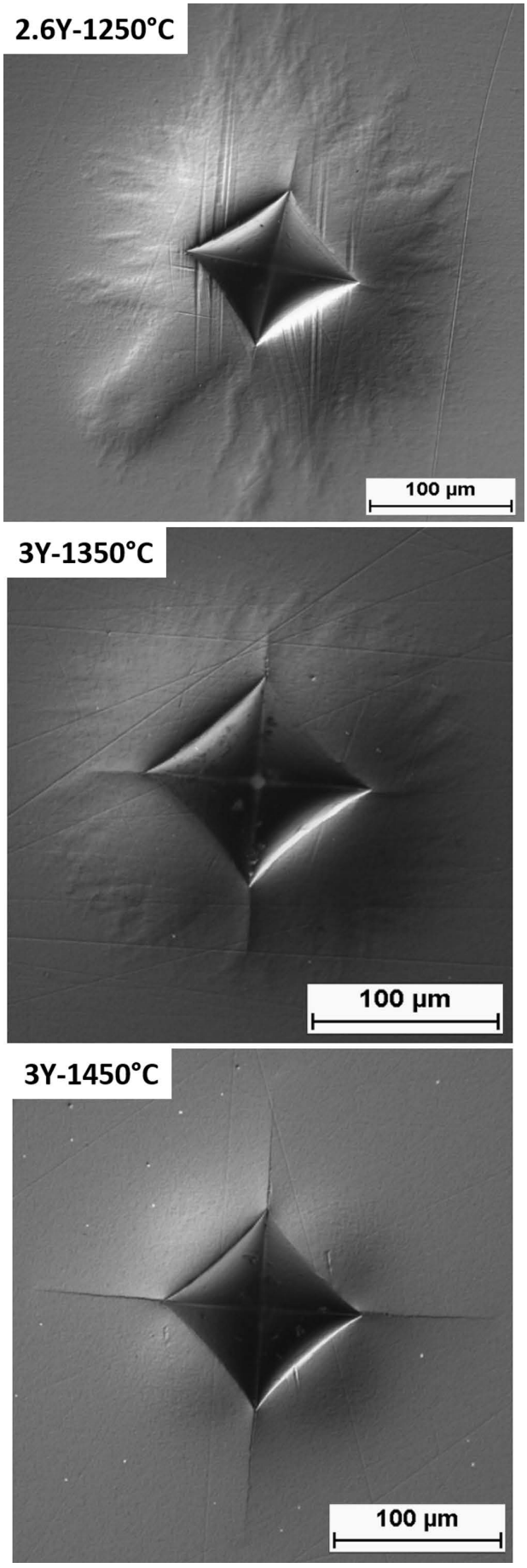

Fig. 4: Crack pattern, and uplift/transformation zones around HV10 indents in three typical Y-TZP materials, optical microscope images using differential interference contrast DIC.

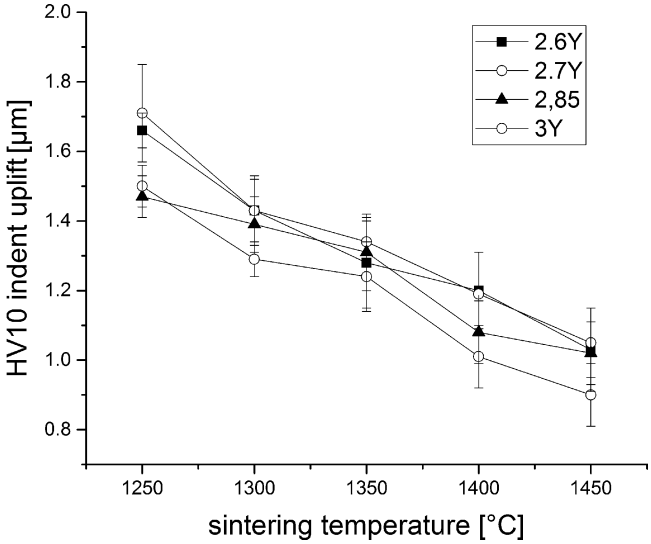

Fig. 5: Height of uplift zones around HV10 indents of the Y-TZPs depending on stabilizer content and sintering temperature, measurement by white light interferometry.

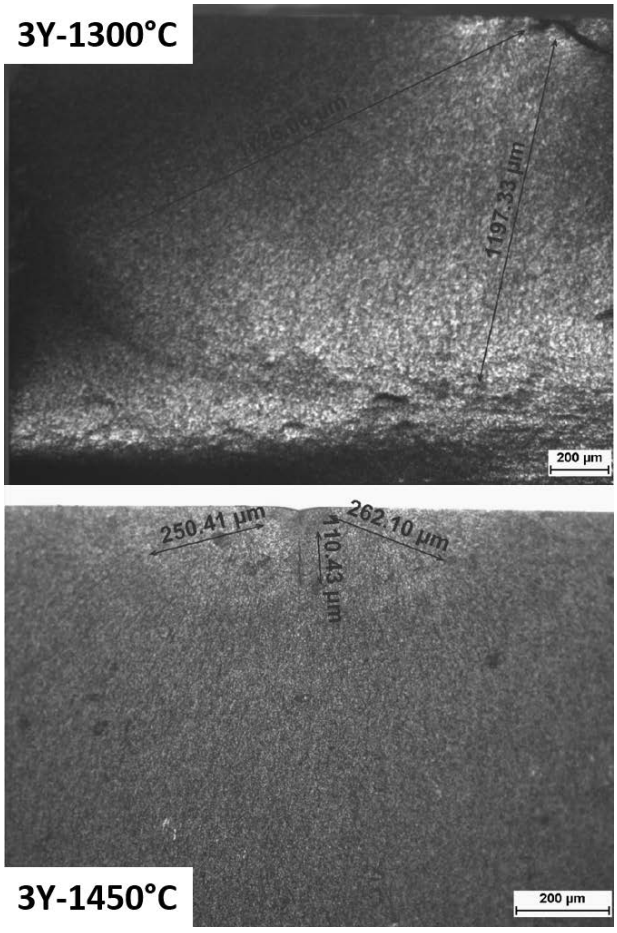

Fig. 6: Subsurface structures of high (3Y-1300 °C) and low toughness (3Y-1450 °C) samples indented by HV10 fractured in ISB test. Images show halos of Palmqvist type indentation cracks and the region of stable crack growth.

merge below the indent, forming a D-shaped pattern. The most surprising fact is how far the stable crack growth zone extends. Depending on the crack growth direction, cracks become critical at a length of up to ~ 1.2 mm in perpendicular and ~ 1.7 mm in lateral direction. However, this

means that the indentation-based crack reaches the outer limits of the sample before the crack has run straight through the specimen. At the compressive side, the formation of a ledge is very uncommon for notched specimens. Fracture resistance and threshold toughness determination with the SIGB method faces some difficulties (in fact it was not possible at all for 2.6Y owing to irregular crack patterns) which, however, have been addressed in previous works dealing with extremely tough TZP materials [24, 34]. The kink in the SIGB plot indicating the value of $K_{app,0}$ which is the R-curve-dependent part of toughness can be identified without difficulty. Fig. 7 plots $K_{app,0}$ values for compositions 2.7Y – 3Y. Again, a distinct difference between samples with high and low stabilizer contents is observed. 2.85Y and 3Y show maxima at intermediate sintering temperatures and a significant decline at higher sintering temperature. 2.7Y shows even a slight increase at higher temperatures. The values measured for the lowest sintering temperatures should not be overstressed. For none of the samples was it possible to determine K_{IC} based on linear extrapolation as the number of data points in the linear section was insufficient (not shown here). Long cracks do form as shown in Fig. 5, but owing to the small sample size and the fast growth they are almost impossible to "catch". Even in cases where long cracks were formed the ascending branch of the SIGB plot was either non-linear or extrapolations led to unrealistically high values of 15 – 20 MPa√m (as described in detail in [30]). It was therefore decided to use K_{ISB} instead of K_{IC} in a more conservative approach to calculate K_{I0} ($K_{I0} = K_{ISB}$-$K_{app,0}$). The resulting ISB-based threshold toughness values K_{I0} are plotted in Fig. 8. Highest threshold toughness values of > 6.5 MPa√m are obtained for 2.85Y sintered at 1300 °C and 1350 °C followed by a total breakdown at higher sintering temperatures to a level of 3 MPa√m; this level is typical for coprecipitated 3Y-TZP [14]. 3Y shows a linear decrease of K_{I0} from 6 MPa√m at 1250 °C to 3.8 MPa√m at ≥ 1350 °C. The resistance to subcritical crack growth is constant at 5 MPa√m for 2.7Y for sintering temperatures ≥ 1300 °C.

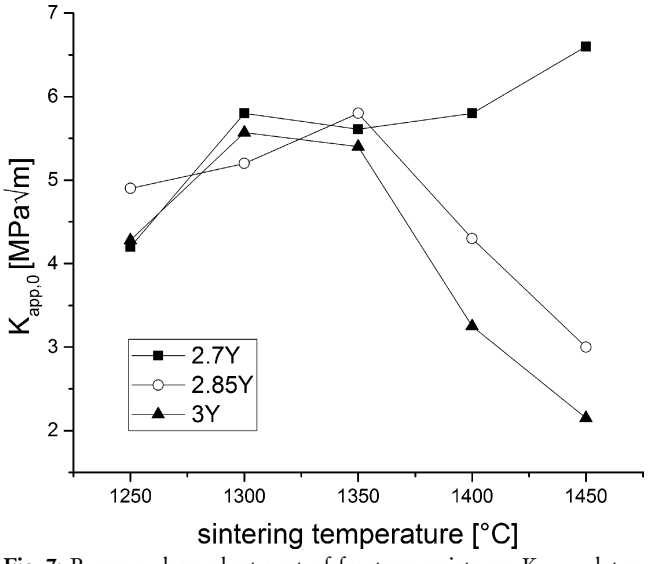

Fig. 7: R-curve-dependent part of fracture resistance $K_{app,0}$ determined by stable indentation crack growth in bending SIGB test for Y-TZPs depending on stabilizer content and sintering temperature.

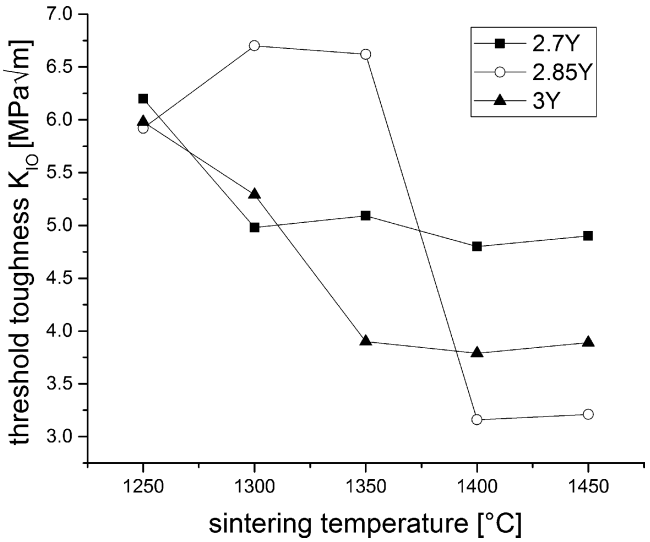

Fig. 8: Resistance to subcritical crack growth K_{I0} determined based on stable indentation crack growth in bending SIGB test for Y-TZPs depending on stabilizer content and sintering temperature.

(2) Phase composition

Fig. 9 shows volumetric monoclinic contents in polished surfaces and ISB fracture faces for different compositions and sintering conditions. Two clear basic trends can be observed. Monoclinic contents in both surfaces decline with rising sintering temperature. Evidently, materials containing more stabilizer have slightly lower monoclinic contents in the polished surface and fracture face, however, it is surprising that for low sintering temperatures this difference is only incremental. As $V_{m,FF}$ declines faster than $V_{m,pol}$ the difference between these values, the transformability V_f also declines with increasing sintering temperature. From a value of initially 45 % at 1250 °C to 15 – 30 % depending on stabilizer content. For the materials containing higher stabilizer content ≥ 2.85 mol% the decrease in transformability at temperatures > 1350 °C is much more pronounced. Based on these XRD data, the transformation zone sizes h were calculated according to Kosmac [32]. The effect of transformation toughening depends on the size h of transformed zone on both sides of the crack. In Fig. 10, it can be seen that for low sintering temperatures all samples reach transformation zone sizes h of ~ 4.5 µm. The following decline of h depends – as we may suspect from toughness and XRD data – on sintering temperature and stabilizer content. For 3Y we observe an almost linear decline to h = 1.5 µm. The compositions containing more stabilizer show a plateau region before a significant reduction of h can be observed. 2.7Y is the exception to the rule here, h stabilizes at 3 µm. With the measured values of V_f, E, ν, constant values for $\varepsilon_T = 0.05$ and X = 0.27 and the calculated value of h the transformation toughness increments $\Delta K_{IC}{}^T = X \cdot 1/(1-\nu) \cdot E \cdot \varepsilon_T \cdot V_f \cdot \sqrt{h}$ can be calculated for the individual compositions [33]. As can be expected, the transformation toughness increments $\Delta K_{IC}{}^T$ shown in Fig. 11 are highest for the lowest sintering temperatures, here all samples reach transformation

toughness values of 3.5 – 4.2 MPa√m. With rising sintering temperatures, transformation toughness in 3Y declines linearly to 1 MPa√m at 1450 °C while the onset of decline is postponed to 1300 – 1350 °C for all other compositions.

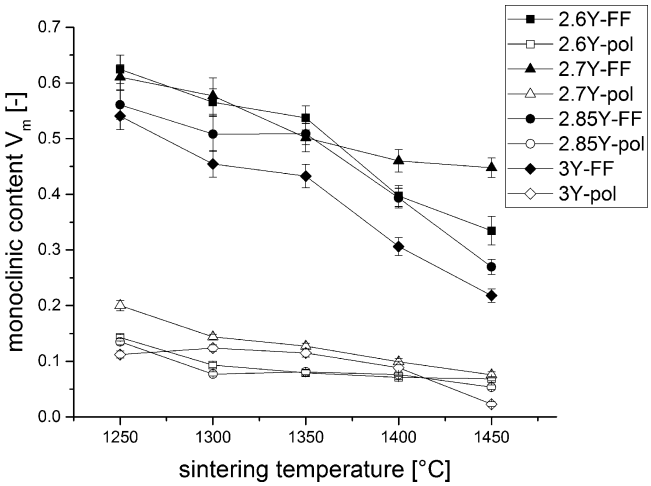

Fig. 9: Monoclinic contents $V_{m,pol}$ in polished surfaces and $V_{m,FF}$ in fracture surfaces of Y-TZPs depending on stabilizer content and sintering temperature.

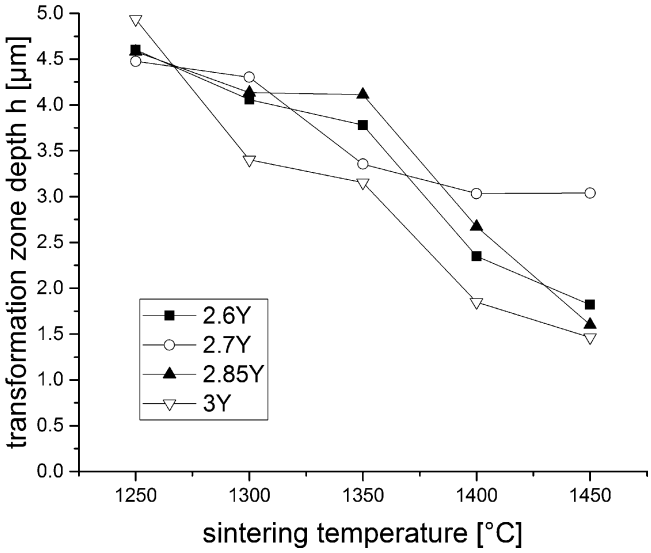

Fig. 10: Calculated transformation zone sizes h of Y-TZPs depending on stabilizer content and sintering temperature.

(3) Microstructure

Fig. 12 shows typical example microstructures of polished surfaces and fracture faces of 3Y samples sintered at 1300 °C and 1450 °C. Prima facie, few differences are visible between samples containing different amounts of stabilizer (not shown) while the influence of grain growth with rising sintering temperature is obvious. Materials sintered at low temperature ≤ 1350 °C stay extremely fine-grained (d ≤ 170 – 190 nm). A closer look and a quantitative evaluation of grain sizes with the line intercept method confirms this sintering-temperature-dependent trend (Fig. 13) but also reveals a weaker dependence. It seems that grain size is only incrementally lower for higher stabilizer contents up to 1400 °C. At the final temperature, a very drastic increase in grain size can be observed, which is most pronounced for the materials containing the lowest stabilizer contents. They reach average grain sizes d of almost 400 nm at 1450 °C.

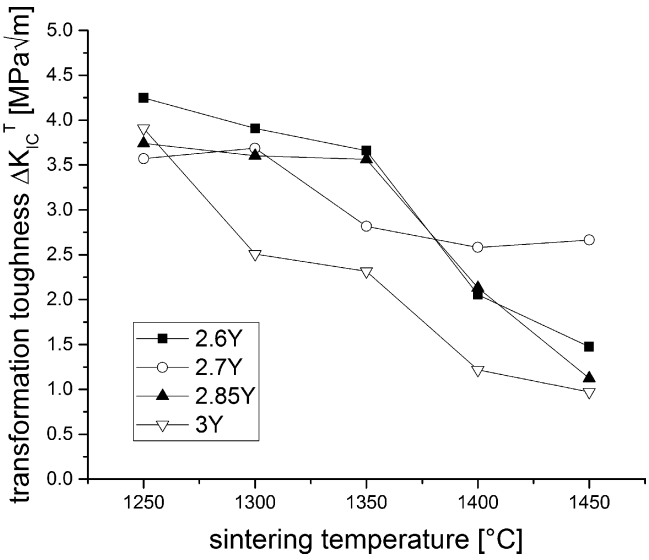

Fig. 11: Calculated transformation toughness increments $\Delta K_{IC}{}^T$ of Y-TZPs depending on stabilizer content and sintering temperature.

IV. Discussions

The results collected in this study present strong evidence in favor of a gradient model to explain the higher toughness of Y-TZP made from coated (compared to coprecipitated) powder provided that the sintering temperature is kept low.

When starting from unstabilized zirconia with a coating or fine dispersion of yttria, interdiffusion of yttria into the zirconia grains begins as soon as the eutectoid phase boundary at 1150 °C is passed as shown by Burger in high-temperature XRD measurements [19]. *A priori* yttria distribution in the grains thus depends on temperature, dwell and initial size of the monoclinic grains. As all yttria is outside the grain at the start, the maximum yttria content in the bulk is limited to the composition that prevails at the t/t+c phase boundary at a given temperature. It can be expected that initially the core of the grains will have an yttria-deficient composition, which makes the bulk tetragonal grains very transformable, at low sintering temperatures we can also expect regions that contain too little yttria to keep the tetragonal phase metastable and will form intragranular monoclinic domains upon cooling. Such almost yttria-free regions have been identified by Ohnishi in STEM studies [35]. Such monoclinic intragranular domains would exert a compressive stress on the grain boundaries and impede the failure by intergranular fracture typical for Y-TZP. This is a scenario similar to the case of intragranular SiC in alumina as discussed by Ferroni and Pezzotti [36]. This would also mean an increase in non-R-curve-dependent toughness i.e. "intrinsic toughness". The shell of the grains containing more yttria requires high stress to be transformed and, as stress-induced phase transformation will start at the grain boundaries rather than in the bulk, ensures high strength despite high toughness and transformability. The fact that all materials have very similar

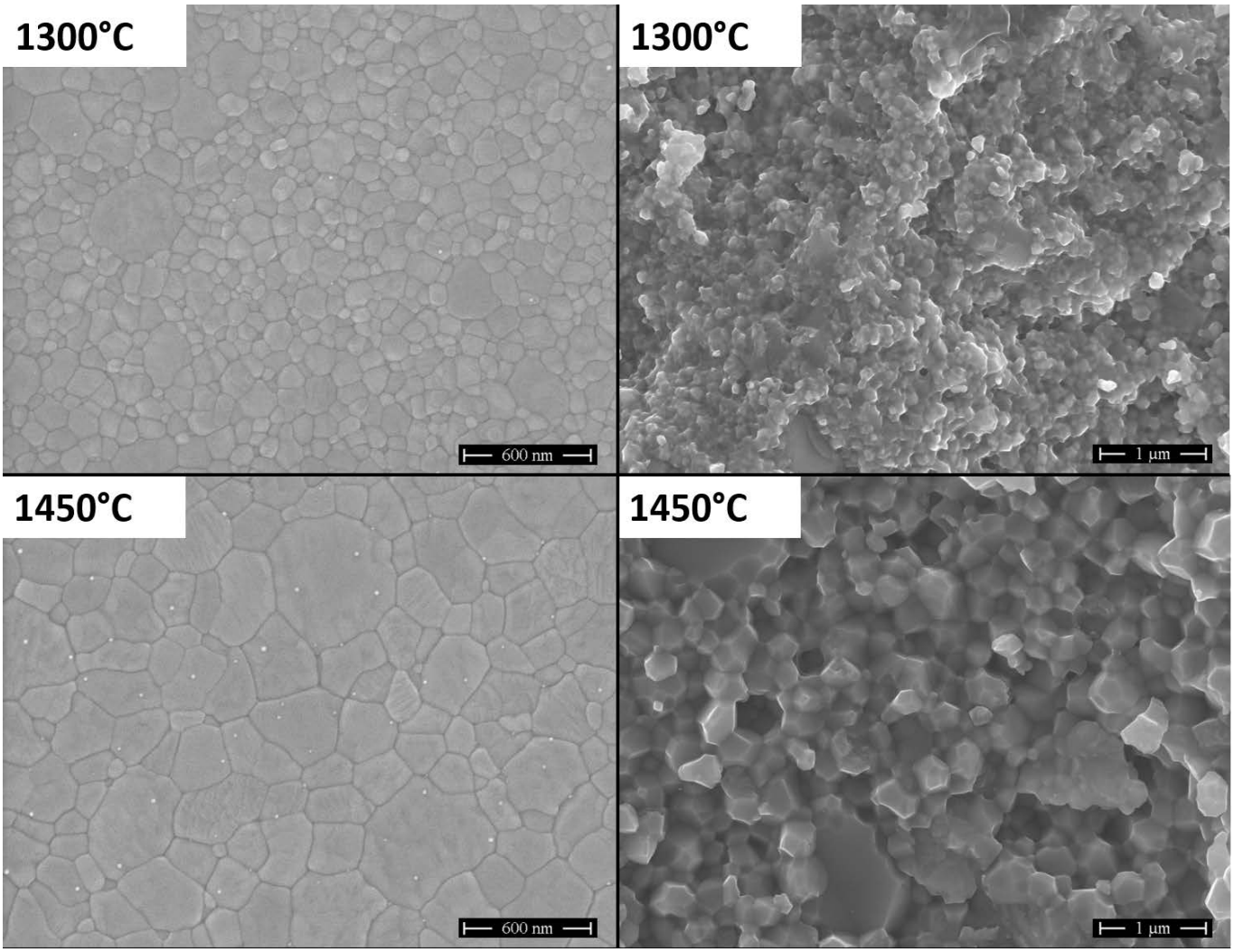

Fig. 12: SEM images of polished and etched as well as fracture faces of 3Y-1300 °C and 3Y-1450 °C.

properties at low sintering temperatures is another indication for the gradient theory as the concentration difference from bulk to surface is identical at the beginning, in the grains an initially identical stabilizer gradient will be formed and it probably does not matter how much excess yttria is at the surface. The superfluous yttria will either stay in the supersaturated grain boundary for which the thermodynamic conditions are different or will separate into cubic grains which are detectable in the microstructure. In the hot press at sintering temperatures of 1250 – 1450 °C the materials are entirely tetragonal (+cubic). Monoclinic domains inside the tetragonal grains form during cooling of the sample to room temperature, their martensite start temperature will depend on the yttria concentration, the temperature and the constraint/Young's modulus of the surrounding matrix (which is constant for plain Y-TZP) [37, 38]. This assumption is supported by the fact that the monoclinic disappears in the case of more rigid matrix systems containing larger amounts of alumina [26, 27]. Monoclinic grains were not detected in SEM, which supports the assumption that these monoclinic regions are intragranular and relatively small (30 – 50 nm).

This core-shell structure will break down at higher sintering temperatures owing to two effects: Progressive interdiffusion of yttria until the saturation limit is reached and grain growth. During grain growth, a part of yttria-rich shell material of the original grains is transported into the bulk when grains merge and will equilibrate the concentration gradients in the bulk. Finally, at higher sintering temperatures we can expect similar conditions as in the case of coprecipitated powder, in fact the strength toughness correlations in coated 3Y-TZP are comparable to state-of-the-art 3Y-TZP (fair toughness, high strength). In the case of Y-TZPs with yttria contents close to the composition at the t/t+c at sintering temperature (~ 2.5 mol%), there is little yttria left at the grain boundaries once the grains are saturated. This together with the larger grain sizes of samples containing low amounts of yttria facilitates transformation, keeps toughness relatively high and limits strength.

The measured phase compositions, visible characteristics of transformation upon indentation and measured fracture resistance values all fit perfectly into this interpretation. The maximum transformation toughness increments of ~ 4.5 MPa$\sqrt{m}$ and transformation depth of h = 4.5 – 5 µm measured for the samples are well in line with the value of ~ 5 MPa$\sqrt{m}$ and ~ 8 µm calculated by Swain as the upper limits possible in Y-TZP [39]. These values were calculated by Swain for the purely dilatoric case X = 0.22, for X > 0.22 (typically X = 0.27 for Y-TZP [1]) transformation

zone h decreases approximately to the measured values [39]. The fact that stress-strain curves show no or only incremental signs of non-linearity at the samples bearing the highest stress does not necessarily mean that they follow the rules of linear fracture mechanics for brittle materials, it may also mean that the samples fail when or shortly after the critical transformation stress of the zirconia is reached.

We may expect – as shown in earlier publications [25, 27] – that the materials retaining a stabilizer gradient and intragranular monoclinic domains and showing toughness values of > 10 MPa√m probably have a higher intrinsic toughness K_0 of > 6 MPa√m (not to be confused with K_{I0} despite similar values!) than coprecipitated materials (4 MPa√m [12]). The R-curve-dependent part of fracture resistance $K_{app,0}$ is higher than the transformation toughness calculated using a value of X = 0.27. Thus either the transformation in these Y-TZP materials is more efficient (X > 0.27) or other toughening mechanisms besides transformation toughening such as microcracking are active. Microcracking is not very likely in ultrafine-grained Y-TZP ceramics with high stabilizer content but may play a role in case of the understabilized materials sintered at high temperature which keep their higher toughness despite moderate transformation toughness.

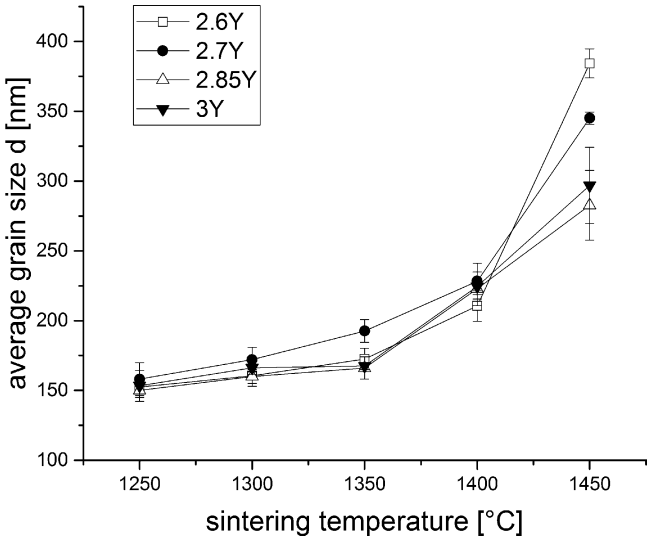

Fig. 13: Grain sizes determined with the line intercept method using a correction factor of 1.54 for Y-TZPs depending on stabilizer content and sintering temperature.

Argumentation on the basis of the toughness measurements presented above still contains a large degree of uncertainty as all toughness measurement protocols known to determine fracture resistance of ceramics have their deficiencies if applied to ultrafine-grained tough and transformable zirconia.

In SEVNB, it is impossible to produce a notch sharp enough (by the accepted standard method) to be in the same order of magnitude as the grain size (< 1.5 – 2 µm). Standard razor blade notches hardly reach radii of less than 10 µm [40]. In a round robin organized by Kuebler even in standard Y-TZP having a grain size of ~ 500 nm strongly diverging toughness values were measured depending on the experimental skills in notching [41]. Direct crack length measurements (DCM) based on Vickers indents suffer from a non-quantifiable influence of the plastified zone and residual stress superimposed with transformation stress [42]. Moreover, it was clearly shown that in the case of the short cracks developed in the samples fired at low temperature, the entire crack is trapped within the transformation zone, which makes DCM measurements potentially inaccurate. Lockup effects as described by Amazigo [43] were observed in preliminary SIGB tests of the toughest materials when the loading increments were too low (not shown here). In the opinion of the authors, starting from Vickers indents has the advantage of producing an ultimately sharp notch. When starting from indentations, long crack methods are preferred in which the indentation cracks are dragged out of their original position to crack lengths beyond the size of the transformed region. Still as shown in the case of the ISB test (and SIGB which is the same experimental setup) the crack profile is Palmqvist type, ISB toughness calculation are, however, calibrated to median cracks [28]. Thus the measurements are to a certain extent more qualitative than quantitative, it can be shown that the materials are very tough, absolute values are still to be discussed. It may even be that materials are tougher than measured owing to the fact that the stable crack length can extend to the edge of a specimen of 2 x 4 mm diameter. In the case of the maximum toughness samples of 2.85Y residual strength values of > 900 MPa were measured in ISB tests which are as high as the average 4pt bending strength, still all samples failed at indents. The idea to remove the plastified zone of the indent by grinding, lapping or polishing to carry out surface crack in flexure (SCF) tests [44] – a method which works quite accurately in the case of brittle materials and has become very accurate after reevaluation of the Newman-Raju Formula [45] – will not work, as together with the plastified zone the entire very shallow crack profile of the toughest samples would be removed.

As long as this toughness issue is not solved satisfactorily. further mechanistic discussions concerning the transformation efficiency are in vain.

In any case for practical application, the Y-TZP materials made from coated nanopowders are an excellent alternative to conventional coprecipitated Y-TZP as – if properly processed – they provide high strength together with high fracture resistance. This makes them reliable and damage-tolerant in respect of single catastrophic events and thus attractive for applications such as dental implants. High K_{I0} values ensure that despite their high toughness the materials are not prone to fatigue up to loads of $\sigma_{fatigue} = \sigma_{4pt} \cdot K_{I0}/K_{IC} = 500$ MPa. As Burger and Zhang have shown such materials have superior ageing resistance [19, 46]. Besides these classical applications, tough Y-TZPs are also interesting matrix materials for composite ceramics.

V. Conclusions

In this study on Y-TZP materials made from stabilizer-coated zirconia powder, a broad range of sintering temperatures and stabilizer contents was covered. Hot pressing provided the advantage of making fully dense materials even at very low sintering temperatures. Thus the evo-

lution of trends in mechanical properties, phase compositions and microstructures become accessible in a sintering temperature range in which pressureless sintering does not lead to dense samples.

In respect of sintering temperature, Y-TZP made from coated powders leads to inverse strength toughness relations than in Y-TZP made from coprecipitated powders. Transformability and thus toughness are high at low sintering temperatures while strength increases with sintering temperature and declining fracture resistance. Toughness in these "coated" Y-TZPs is thus not related to stabilizer content and grain size alone but presumably a result of a complex process of thermally activated interdiffusion of yttria into the bulk, grain growth and retaining of intragranular monoclinic domains exerting residual stress. Once the problem of accurate measurement of fracture resistance is solved, a conclusive modelling of the materials may become available. Further issues to be addressed in the future are the influence of different starting powders and a study of the Y-TZP materials in an even narrower grid of parameters composition, temperature, dwell and stabilizer concentration. Detailed TEM analyses may provide more quantitative evidence on the kinetics of stabilizer interdiffusion.

Acknowledgements

The authors would like to express their gratitude to Felicitas Predel and Willi Schwan for their assistance in SEM and microscopy. This research did not receive any specific grant from funding agencies in the public, commercial, or not-for-profit sectors.

References

[1] Kelly, P.M., Rose, L.R.F.: The martensitic transformation of ceramics – its role in transformation toughening, *Progr. Mater. Sci*., **67**, 463 – 557, (2002).

[2] Hannink, R.H.J., Kelly, P.M., Muddle, B.C.: Transformation toughening in zirconia-containing ceramics, *J. Am. Ceram. Soc*.,**83**, 461 – 487, (2002).

[3] Lai, T.R., Hogg, C.L., Swain, M.V.: Evaluation of fracture toughness and R-curve behaviour of Y-TZP ceramics, *ISIJ Int.*, **29**, 240 – 245, (1989).

[4] Anderson, R.M., Braun, L.M.: Technique for the R-curve determination of Y-TZP using indentation-produced flaws, *J. Am. Ceram. Soc.*, **73**, 3059 – 3062, (1990).

[5] Chen, M., Hallstedt, B., Gauckler, L.: Thermodynamic modeling of the ZrO_2-$YO_{1.5}$ system, *Solid State Ionics*, **170**, 255 – 274, (2004).

[6] Li, P., Chen, I.W., Penner-Hahn, J.: Effect of dopants on zirconia stabilization - an X-ray absorption Study: I, trivalent dopants, *J. Am. Ceram. Soc.*, **77**, 118 – 128, (1994).

[7] Schmauder, S., Schubert, H.: Significance of internal stresses for the martensitic transformation in yttria-stabilized tetragonal zirconia polycrystals during degradation, *J. Am. Ceram. Soc.*, **69**, 534 – 540, (1986).

[8] Sagel-Ransijn, D.D., Winnubst, A.J.A., Burggraaf, A.J., Verweij, H.: Grain growth in ultrafine-grained Y-TZP ceramics, *J. Eur. Ceram. Soc*., **17**, 1133 – 1141,(1997).

[9] Matsui, K., Horikoshi, H., Ohmichi, N., Ohgai, M., Yoshida, H., Ikuhara, Y.: Cubic-formation and grain-growth mechanisms in tetragonal zirconia polycrystal, *J. Am. Ceram. Soc.*, **86**, 1401 – 1408, (2003).

[10] Chevalier, J., Gremillard, L., Deville, S.: Low temperature degradation of zirconia and implications for biomedical implants, *Annu. Rev. Mater. Res.*, **37**, 1 – 32, (2007).

[11] Ruiz, L., Readey, M.J.: Effect of heat treatment on grain size, phase assemblage, and mechanical properties of 3 mol% Y-TZP, *J. Am. Ceram. Soc.*, **79**, 2331 – 2340 (1996).

[12] Swain, M.V., Rose, L.R.F.: Strength limitations of transformation-toughened zirconia alloys, *J. Am. Ceram. Soc.*, **69**, 511 – 518, (1986).

[13] Wroe, S., Ferrara, T.L., McHenry, C.R., Curnoe, D., Chamoli, U.: The cranio-mandibular mechanics of being human, *P. Roy. Soc. B-Biol. Sci.*, **277**, 3579 – 3586 (2010).

[14] Chevalier, J., Saadaoui, M., Olagnon, C., Fantozzi, F.: Double-torsion testing a 3Y-TZP ceramic, *Ceram. Int.*, **22**, 171 – 177, (1996).

[15] Swain, M.V.: Grain-size dependence of toughness and transformability of 2 mol% Y-TZP ceramics, *J. Mater. Sci. Lett.*, **5**, 1159 – 1162, (1986).

[16] Danilenko, I., Konstantinova, T., Volkova, G., Burkhovetski, V., Glazunova, V.: The role of powder preparation method in enhancing fracture toughness of zirconia ceramics with low alumina amount, *J. Ceram. Sci. Tech.*, **6**, 191 – 200, (2015).

[17] Lange, F.F.: Transformation toughening – part 3: experimental observations in the ZrO_2-Y_2O_3 system, *J. Mater. Sci.*, **17**, 240 – 246, (1982).

[18] Singh, R., Gill, C., Lawson, S., Dransfield, G.P.: Sintering, microstructure and mechanical properties of commercial Y-TZPs, *J. Mater. Sci.*, **31**, 6055 – 6062, (1996).

[19] Burger, W., Richter, H.G., Picconi, C., Vatteroni, R., Cittadini, A., Boccalari, M.: New Y-TZP powders for medical grade zirconia, *J. Mater. Sci. – Mater. M.*, **8**, 113 – 118, (1997).

[20] Yuan, Z.X., Vleugels, J., Van der Biest, O.: Preparation of Y_2O_3-coated ZrO_2 powder by suspension drying, *J. Mater. Sci. Lett.*, **19**, 359 – 361, (2000).

[21] Ohnishi, H., Naka, H., Sekino, T., Ikuhara, Y., Niihara, K.: Mechanical properties of 2.0 – 3.5 mol% Y_2O_3-stabilized zirconia polycrystals fabricated by the solid phase mixing and sintering method, *J. Ceram. Soc. Jpn.*, **116**, 1270 – 1277, (2008).

[22] Kern, F.: Alumina-doped 2.5Y-TZP produced from yttria-coated pyrogenic nanopowder, *J. Ceram. Sci. Tech.*, **2**, 89 – 96, (2011).

[23] Vleugels, J., Xu, T., Huang, S., Kan, Y., Wang, P., Li, L., Van der Biest, O.: Characterization of (Nd,Y)-TZP ceramics prepared by a colloidal suspension coating technique, *J. Eur. Ceram. Soc*., **27**, 1339 – 43, (2007).

[24] Kern, F.: Ytterbia-neodymia-costabilized TZP–Breaking the limits of strength–toughness correlations for zirconia?, *J. Eur. Ceram. Soc*., **33**, 965 – 973, (2013).

[25] Vleugels, J., Yuan, Z.X., Van Der Biest, O.: Mechanical properties of Y_2O_3/Al_2O_3-coated Y-TZP ceramics, *J. Eur. Ceram. Soc*., **22**, 873 – 881, (2002).

[26] Kern, F., Gadow, R.: Alumina toughened zirconia from yttria coated powders, *J. Eur. Ceram. Soc*., **32**, 3911 – 3918, (2012).

[27] Kern, F., Gadow, R.: Mechanical properties and low temperature degradation resistance of 2.5Y-TZP – alumina composites, Materiały Ceramiczne/Ceramic Materials, **65**, 258 – 266, (2013).

[28] Chantikul, B., Anstis, G.R., Lawn, B.R., Marshall, D.B.: A critical evaluation of indentation techniques for measuring fracture toughness: II, Strength method, *J. Am. Ceram. Soc.*, **64**, 539 – 543, (1989).

[29] Dransmann, G.W., Steinbrech, R.W., Pajares, A., Guiberteau, F., Dominguez-Rodriguez, A., Heuer, A.: Indentation studies on Y_2O_3-stabilized ZrO_2: II, Toughness determination from stable growth of indentation-induced cracks, *J. Am. Ceram. Soc.*, **77**, 1194 – 1201, (1994).

[30] Lube, T., Fett, T.: A threshold stress intensity factor at the onset of stable crack extension of knoop indentation cracks, *Eng. Fract. Mech.*, **71**, 2263 – 2269, (2004).

[31] Toraya, H., Yoshimura, M., Somiya, S.: Calibration curve for quantitative analysis of the monoclinic-tetragonal ZrO_2 system by X-ray diffraction, *J. Am. Ceram. Soc.*, **67**, C119 – C121, (1984).

[32] Kosmac, T., Wagner, R., Claussen, N.: X-ray determination of transformation depths in ceramics containing tetragonal ZrO_2, *J. Am. Ceram. Soc.*, **64**, C72 – C73, (1981).

[33] McMeeking, R.M., Evans, A.G.: Mechanics of transformation-toughening in brittle materials, *J. Am. Ceram. Soc.*, **65**, 242 – 246, (1982).

[34] Kern, F.: A comparison of microstructure and mechanical properties of 12Ce-TZP reinforced with alumina and in situ formed strontium- or lanthanum hexaaluminate precipitates, *J. Eur. Ceram. Soc.*, **34**, 413 – 423, (2013).

[35] Ohnishi, H., Fukuhara, T., Kawanami, T., Sekino, T., Ikuhara, Y., Niihara, K.: Microstructure and crystal phase development of Y_2O_3 stabilized zirconia polycrystal fabricated by the solid phase mixing and sintering method, *J. Ceram. Soc. Jpn.*, **115**, 210 – 215, (2007).

[36] Ferroni, L.P., Pezzotti, G.: Evidence for bulk residual stress strengthening in Al_2O_3/SiC nanocomposites, *J. Am. Ceram. Soc.*, **85**, 2033 – 2038, (2002).

[37] Becher, P.E., Alexander, K.B., Bleier, A., Waters, S.B., Warwick, W.H.: Influence of ZrO_2 grain size and content on the transformation response in the Al_2O_3-ZrO_2 (12 mol% CeO_2) system, *J. Am. Ceram. Soc.*, **76**, 657 – 663, (1993).

[38] Lange, F.F.: Transformation toughening – Part 1: Size effects associated with the thermodynamics of constrained transformations, *J. Mater. Sci.*, **17**, 225 – 234, (1982).

[39] Swain, M.V.: Limitation of maximum strength of zirconia-toughened ceramics by transformation toughening increment, *J. Am. Ceram. Soc.*, **68**, C97 – C99, (1985).

[40] Fischer, H., Waindich, A., Telle, R.: Influence of preparation of ceramic SEVNB specimens on fracture toughness testing results, *Dent. Mater.*, **24**, 618 – 624, (2008).

[41] Kuebler, J.: Fracture toughness of ceramics using the SEVNB method; round robin, in: R. C. Bradt, D. Munz, M. Sakai, V. Ya. Shevchenko, K. White (Eds.) Fracture mechanics of ceramics 13, Kluwer Academic, Dordrecht, 2002, 437 – 445.

[42] Quinn, G.D., Bradt, R.C.: On the vickers indentation fracture toughness test, *J. Am. Ceram. Soc.*, **90**, 673 – 680, (1997).

[43] Amazigo, J.C., Budiansky, B.: Interaction of particulate and transformation toughening, *J. Mech. Phys. Solids*, **36**, 581 – 595. (1988).

[44] Morrell, R.: Fractography and fracture toughness measurement, *Key Eng. Mat.*, **409**, 17 – 27, (2009).

[45] Strobl, S., Supancic, P., Lube, T., Danzer, R.: Surface crack in tension or in bending – A reassessment of the newman and raju formula in respect to fracture toughness measurements in brittle materials, *J. Eur. Ceram. Soc.*, **32**, 1491 – 1501, (2012).

[46] Zhang, F., Vanmeensel, K., Inokoshi, M., Batuk, M., Hadermann, J., van Meerbeek, B., Naert, I., Vleugels, J.: 3Y-TZP ceramics with improved hydrothermal degradation resistance and fracture toughness, *J. Eur. Ceram. Soc.*, **34**, 2453 – 63, (2014).